https://doi.org/10.5194/gchron-2021-32
Preprint. Discussion started: 3 November 2021

Technical note: Quantifying Uranium-series disequilibrium in natural samples for dosimetric dating - Part 1: gamma spectrometry

Barbara Mauz[1,2], Paul J. Nolan[3], Peter G. Appleby[3],

[1] School of Environmental Sciences, University of Liverpool, Liverpool, L69 7ZT, UK
[2] Department of Geology and Geography, University of Salzburg, Salzburg, 5020, Austria
[3] School of Physical Sciences, University of Liverpool, Liverpool, L69 7ZT, UK

Correspondence to: Barbara Mauz (mauz@liverpool.ac.uk)

Abstract

Dosimetric dating techniques rely on accurate and precise determination of environmental radioactivity. Gamma spectrometry is the method of choice for determining the activity of ^{238}U, ^{232}Th and ^{40}K. With the aim to standardise gamma-spectrometric procedures for the purpose of determining accurate parent nuclide activities in natural samples, we outline here basics of gamma spectrometry and practical laboratory procedures. This includes gamma radiation and instrumentation, sample preparation, finding the suitable measurement geometry and sample size for a given detector and using the most suitable energy peaks in a gamma spectrum. The issue of correct efficiency calibration is highlighted. The procedures outlined are required for estimating contemporary parent nuclide activity. For estimating changing activities during burial specific data analyses are required and these are also highlighted.

1 Introduction

Dosimetric dating is a method for determining the age of objects from accumulated damage to their constituent crystals caused by exposure to radiation, typically from natural radionuclides such as uranium and ^{40}K present in most soils and sediments. It is of critical importance to the dating technique that the quantity of the radiation dose is estimated accurately and this is usually the case when its rate is constant. Because of radioactive decay the dose rate will in many situations vary over time and the most important source for this variation are the ^{238}U series radionuclides, and in particular the short-lived daughters of the intermediate radionuclide ^{226}Ra. Resolution of any initial disequilibrium between ^{226}Ra and its parents will normally take place on millennial time-scales, and so result in significant changes to the dose rate over time. The simplest and most straightforward method for determining activities of ^{226}Ra, its parents and its short-lived daughters is by gamma spectrometry (e.g., Murray and Aitken, 1988). Although the initial set up can be quite demanding, because of its operational simplicity this is increasingly the method of choice (e.g., Murray et al., 2015), particularly where there is evidence of radiometric disequilibrium.

Despite operational simplicity, the interlaboratory comparison (Murray et al., 2015) reveals discrepancies between laboratories that are of great concern. While the exact reasons are unknown, we suspect that problems arise from data analysis, peak interference and self-absorption and from the use of suitable reference material (e.g., Murray et al., 2018) for efficiency calibration. We address these problems in the first part of our paper where we outline the basic principles

https://doi.org/10.5194/gchron-2021-32
Preprint. Discussion started: 3 November 2021

of gamma spectrometry for estimating contemporary dose rates. We show how the degree of isotopic fractionation can be quantified using the approach published in Abdualhadi et al. (2018). For estimating the historical dose rate the radioactive decay equations (the Bateman equations) for the intervening period must be solved (e.g., Degering and Degering, 2020). Analytical solutions of these equations, and software procedures for calculating historical dose rates, will be the subject of the second part of our paper.

2 Gamma radiation and gamma spectrum

Ionizing radiation from atoms undergoing radioactive decay includes both subatomic particles (alpha rays, beta rays), and also electromagnetic waves from the higher end of the energy spectrum (gamma rays, X-rays). Gamma rays are emitted when the decay product undergoes de-excitation from a higher energy level to a lower one, or to the ground state, and are characterised by photon energies in the range 20 keV to 3 MeV. Most of the radionuclides relevant for dosimetric dating emit gamma rays of energies <1 MeV. Gamma rays can penetrate material objects typically to a depth of several centimetres depending on the photon energy and characteristics of the material (in particular its attenuation coefficient), though with an intensity that attenuates exponentially with distance. For example, the intensity of a 1 MeV photon penetrating SiO_2 is reduced for 50% at a penetration depth of 4.7 cm; the intensity is reduced for 63% at 6.8 cm. Values of the attenuation coefficients at other photon energies or for other materials or mixtures can be found in the literature or from online databases (for details see Appendix A).

Although gamma rays make only a small contribution to the radiation dose compared to alpha and beta particles, they play an important role in determining the source and strength of the dose. In contrast to beta particles, gamma photons energies are discrete, and specific to particular nuclides. This allows determination of gamma emitting radionuclides contained within a source from peaks in a gamma ray energy spectrum (Fig. 1) obtained from that source.

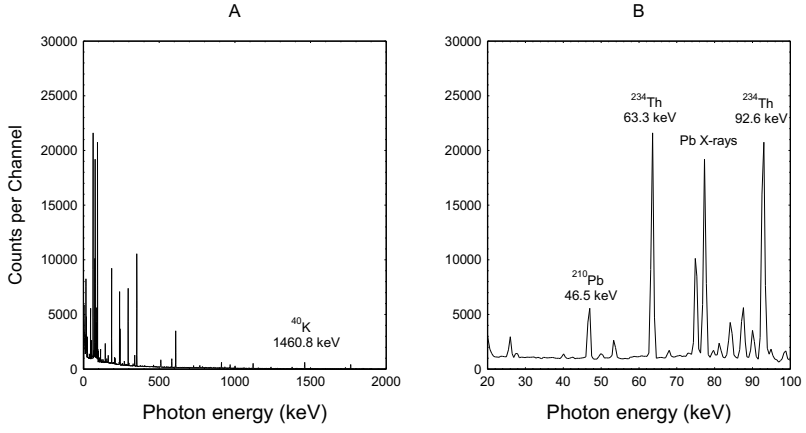

Fig.1. Typical gamma spectra showing the numbers of counts (photon interactions) per channel at energies ranging from A - 20 keV to 2000 keV and B - 20 keV to 100 keV. The dispersion is 2 channels per keV. Peaks in the spectrum identify emissions from specific radionuclides.

3 Detector and instrumentation

https://doi.org/10.5194/gchron-2021-32
Preprint. Discussion started: 3 November 2021

Gamma ray emissions from environmental samples are readily analysed using semiconductor gamma detectors. Electrons displaced by photons traversing the crystal at the heart of the detector are gathered using an applied high voltage, and the total charge collected related to the photon energy. These devices are most commonly constructed using crystals made of high-purity Germanium (HPGe). Near-perfect single crystals of Ge can be produced in a range of different sizes and configurations suitable for analysing environmental samples (for details see Gilmore, 2008). Ge detectors are operated at low temperature to reduce the background current, i.e. charge carriers that are generated due to the relatively low band gap (0.7 eV) of germanium. The typical installation of a HPGe detector includes the detector and preamplifier within the cryostat housing and the nitrogen dewar (Fig. 2A), the shield surrounding the cryostat (Fig. 2B), the amplifier and the multichannel analyser where the latter two are today increasingly replaced by a digital system. The energy range is typically 10-2600 keV.

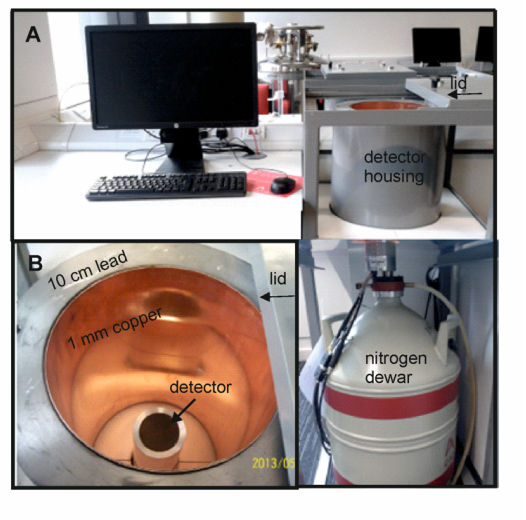

Fig. 2. Typical configuration of a gamma spectrometer with A – detector housing, nitrogen dewar and PC; B – view in the detector housing; the shield is composed of 10 cm low-activity lead, 1mm tin (not visible) and 1mm copper. Amplifier and preamplifier not shown (adopted from Abdualhadi, 2016).

Table 1. Properties of commonly used Ge detectors in terms of diameter, length and peak resolution. FWHM = full width half maximum of energy peak. The efficiency is relative to a sodium-iodide (3x3 inch) detector taken at 25 cm.

Ge Detector Type		Resolution FWHM (keV)					Diameter (mm)	Length (mm)	Rel Efficiency (%) at 1332 keV	Reference
	Energy (keV)	60	90	122	662	1332				
Coaxial (n)		0.80	0.87	0.90	1.20	1.80	60	60	38	Abdualhadi et al. (2018)
BEGe		0.55	0.60	0.65	1.10	1.80	60	25	18	
Coaxial (n)		-	-	0.81	-	1.78	55	45	~20	Murray et al. (2018)
Coaxial (p)		-	-	-	-	1.90	49	30	~10	
Coaxial (n)		0.92	-	0.98	1.39	1.85	61.8	77.8	54	This Study

https://doi.org/10.5194/gchron-2021-32
Preprint. Discussion started: 3 November 2021

Table 1 compares detector specifications. The BEGe (Broad Energy Germanium) detector has a short length and a different electrode geometry compared to the n- and p-type coaxial detectors. It ensures good charge collection and excellent low-energy resolution. On all detectors types samples are placed close to the end cap to ensure good interception of gamma emissions from the sample. At low energy (<200 keV; Abdualhadi et al., 2018) they have a similar efficiency for the same detector diameter, though the better energy resolution of the BEGe detector allows a more precise determination of the peak areas than the coaxial detector. This is important when the low energy gamma rays are a vital part of the analysis. At higher energies the coaxial detector has a significantly better efficiency due to its longer length. The BEGe detector, on the other hand, typically has a lower Compton background in the spectrum as there is less material to scatter high-energy gamma rays such as the 1461 keV from ^{40}K and the 2614 keV from the thorium decay series.

3.1 Interaction between detector and sample

There are interactions occurring between the detector and the sample's gamma rays that are independent of detector configuration and measurement geometry but disturb the recording of the sample's activity. These interactions occur across the energy range of interest with variable significance depending on the average atomic number (Z) of a given sample. In the low-energy region a photon may be absorbed and its energy ejects an electron from its host atom (Photoelectric effect). In the intervening energy region the incoming photon is scattered by an electron resulting in a decrease of the photon's energy (Compton scattering). Photons with energies of 1.022 MeV can cause the formation of an electron and a positron (Pair production).

3.2 Full-energy peak efficiency

Gamma photons entering the detector crystal may be fully absorbed, partially absorbed, or escape interaction altogether. Only those photons that are fully absorbed will contribute to the relevant photo-peak. Full-energy peak efficiency is defined as the ratio of the number of counts detected in a peak to the number emitted by the source. Its value for any given photon energy will depend on the properties of the detector and the configuration of the sample. Fig. 3 shows plots of efficiency versus photon energy for two of the detectors listed in Table 1. These were determined using standard sources of known activity. While both detectors have similar efficiency at low energy, the coaxial detector has a significantly higher efficiency as the gamma-ray energy increases due to its longer length. In both detectors, the practical efficiency at low gamma-ray energies can be reduced by other effects such as self-absorption of photons within the sample (see sec. 6.2).

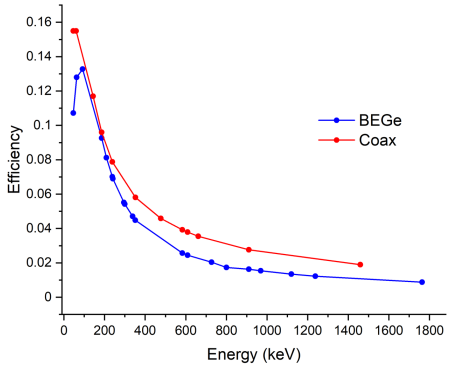

Fig. 3. Typical efficiency data for two detectors with diameters close to 60 mm. Data were determined with samples in the form of discs covering the front face of the detector. Samples have a diameter of 60 mm and a thickness of 13 mm. Data were normalised at low energy to account for the small difference in diameter of the two detectors. See Table 1 for description of BEGe and Coaxial (n) of this study.

https://doi.org/10.5194/gchron-2021-32
Preprint. Discussion started: 3 November 2021

4 Sample preparation and measurement geometries

Samples are normally dried and then placed in a suitable sample holder. There are three common measurement geometries: Marinelli beaker, cylindrical pot, and the case of a well-type detector, sample tubes designed to fit snugly in the well (see Appendix B, Fig. B1). To obtain the texture suitable for the relevant measurement geometry samples can be pulverised and homogenised and placed in a geometry that matches that of the standards used to calibrate the detector. One method for achieving this is to mix the dried and powdered sample with wax before casting it in a shape matching the required geometry (Fig. B2). Since some radionuclides may be preferentially selected by certain components within the sample, any treatment should be careful maintain the original composition. Removing a component, for instance organic matter, may generate inaccurate data because different components may be in different stages of equilibrium depending on their geochemical history during burial. If ^{226}Ra is being determined via its short-lived daughter ^{214}Pb the sample will need to be sealed to prevent escape of the intermediate radionuclide ^{222}Rn and stored for ~25 days to ensure ^{226}Ra/^{222}Rn/^{214}Pb radioactive equilibrium.

In practise, the sample configuration will be dictated by the detector type, the amount of available material and the need to minimise self-absorption (see sec 6.2). Although the near 4π geometry makes Marinelli beakers (ca 300 ml volume; see Fig. B1c) the preferred configuration, this will only be practicable where there is sufficient material to completely fill the beaker. Where the amount of material is limited (<100 g), for a coaxial or BEGe detector the most suitable geometry will be cylindrical (Fig. B1a), with a diameter comparable to that of the detector. Well-type tubes (Fig. B1b) can normally only accommodate very small samples, typically no more than a few grams, and are only suitable for use on well-type detectors and where larger amounts of material are not available.

5 Data analysis

Calculations of radionuclide activities need to take into account emission probabilities (see Table 2 for values for ^{238}U series radionuclides and Table 3 for the ^{232}Th series), full-energy peak efficiency (e.g., Fig. 3), geometry-dependent true coincidence summing (see Gilmore, 2008 for details), background characteristics of the detector (see Appendix C for details), interactions between sample and detector and measurement geometry. Table 2 lists photon energies and emission probabilities for key members of the ^{238}U series (see Guibert et al., 1994 for comparison). Table 3 lists corresponding values for key members of the ^{232}Th series. For radionuclides with multiple energy lines, a best value of the activity may be obtained by using a weighted sum of activities determined from each of the most suitable lines. The other main natural source, ^{40}K, emits 1460.8 keV photons with a probability of 10.66 ± 0.16 %. The peak area given by most software will include background counts as well as those due to emissions from the sample itself. The number of counts in a peak is most easily measured when the peak is well resolved, stands alone free from the interference of any neighbouring peak, and has a small background contribution. Methods for calculating the peak area may include a simple summation of counts in channels within the region of interest or use a procedure such as the Levenberg-Marquardt Nonlinear Least Squares Fit algorithm for fitting the peak to a prescribed shape.

https://doi.org/10.5194/gchron-2021-32
Preprint. Discussion started: 3 November 2021

Table 2. Key gamma emitting ^{238}U series radionuclides, their emission energies (Eγ) and emission probabilities (Pγ). The ^{234}Th peak at 63.3 keV is a doubleton that includes emissions at two different energy levels, 62.9 keV (0.016%) and 63.3 keV (3.7%). The peak at 92.6 keV includes emission at three different energy levels, at 92.3 keV (0.017%), 92.4 keV (2.12%) and 92.8 keV (2.10%). Data are from the National Nuclear Data Centre (www. nndc.bnl.gov).

Radionuclide	E_γ (keV)	P_γ (%)	Uncertainty (keV)	Rel Uncertainty (%)
^{234}Th	63.3	3.70	0.40	10.8
	92.6	4.23	0.28	6.6
^{226}Ra	186.2	3.64	0.04	1.1
^{214}Pb	295.2	18.42	0.04	0.2
	351.9	35.60	0.07	0.2
^{214}Bi	609.3	45.49	0.16	0.4
	1120.3	14.92	0.03	0.2
	1764.5	15.30	0.03	0.2
^{210}Pb	46.5	4.25	0.04	0.9

160

Table 3. Radioisotopes suitable for determining the ^{232}Th activity, their emission energies (E_γ) and emission probabilities (P_γ). Data are from the National Nuclear Data Centre (www. nndc.bnl.gov).

Radionuclide	E_γ (keV)	P_γ (%)	Uncertainty (keV)	Rel Uncertainty (%)
^{228}Ac	270.25	3.46	0.06	1.7
	328.00	2.95	0.12	4.1
	338.32	11.27	0.19	1.7
	911.20	25.8	0.4	1.6
	968.97	15.8	0.3	1.9
^{208}Tl	583.19	85.0	0.3	0.4
	860.56	12.5	0.1	0.8
^{212}Pb	238.6	43.6	0.5	1.1

In routine measurements peak interferences and non-linear peak efficiencies due to self-absorption can be minimised by
165 (i) limiting sample size (i.e. height of fill in the sample holder, Fig. B1), by (ii) using a reference material of known activity (see sec 5.1 and Appendix C) having exactly the same geometry as the unknown sample and similar self-absorption characteristics, and (iii) using the most reliable energy lines for determining activities (Tables 2 and 3).

https://doi.org/10.5194/gchron-2021-32
Preprint. Discussion started: 3 November 2021

5.1 Efficiency calibration

For environmental samples the calibration method of choice is comparing the unknown sample with a sample of known activity concentration (reference sample). It is of vital importance that reference and unknown samples are similar in terms of atomic number, mass and density and that the measurement geometry is kept constant. This straightforward approach is compromised insofar as available certified reference material (e.g., IAEA, NRCAN; Murray et al, 2018) is typically not ideal in terms of its properties. As a consequence, non-certified reference material specifically established for dosimetric dating is often in use (e.g., De Corte et al., 2007; Preusser and Kasper, 2001). Alternatively, certified material is deployed in concert with a number of variables that account for emission probability, full-energy peak efficiency and, eventually, density or chemical composition. This procedure is specific to the detector and can be established through a series of experiments or it is carried out through software packages provided by the manufacturer (e.g., LabSOCS, ANGLE). For details see Appendix C.

The interlaboratory comparison study published by Murray et al. (2015) show considerable differences for gamma-spectrometric results obtained for ^{238}U and ^{232}Th. Because U and Th constitute around 30% of the total annual dose rate (Aitken, 1985), these differences are of great concern. While some of the differences may arise from procedures carried out in individual laboratories, the efficiency calibration is an issue affecting all laboratories. An empirical study (Mauz et al., in review) suggests that the calibration method contribute <10% differences for the activity data of ^{238}U, ^{232}Th and ^{40}K when unsuitable energy peaks (e.g., 186 keV; see Fig. C1a) are excluded.

5.2 Uncertainties

The uncertainty in the overall result depends on a range of factors. These include counting statistics, detection efficiency, nuclear decay data, sample composition, geometry-defined true coincidence summing etc.

For the typical activities to be measured and the samples sizes used the uncertainty arising from counting statistics is typically 2-5% for a counting time of around 1 day. This depends on the intensities of the various gamma rays used in the analysis. The detection efficiency depends in the counting geometry and the detector used, it also varies with gamma-ray energy. By using a series of different reference materials to fully characterise the systems used an uncertainty of 2-3% can be achieved. The emission probabilities obtained from the nuclear decay data have uncertainties. Tables 2 and 3 show that the majority of these are small. The exception is the decay of ^{234}Th. Here the two gamma rays have relatively large uncertainties. If both can be used in the analysis then the uncertainty for ^{234}Th is around 5%. The sample composition can lead to self-absorption particularly for low energy gamma rays. When the density of the sample is known as well as its elemental composition the amount of self-absorption can be determined accurately with an uncertainty of only a few percent. The effect of true coincidence summing also needs to be taken into account. This depends on the decay scheme of the nuclei involved and the detection efficiency of the system being used. For most of the nuclei in the uranium and thorium decay chains this effect is very small for the efficiencies that are used in the majority of counting geometries and is not a major contributor to uncertainty. For more details see Abdualhadi (2016). Overall, uncertainties of 3 – 6 % can be achieved.

6 Quantifying U-series radionuclides for the detection of secular disequilibrium

In samples that have effectively been sealed for long periods of time, members of the ^{238}U series will all be in radioactive equilibrium, that is, they will all have the same activity. In this case the activity can in principle be determined using

https://doi.org/10.5194/gchron-2021-32
Preprint. Discussion started: 3 November 2021

any of the 9 photo peaks listed in Table 2. In practice, mobilisation of intermediate member is likely to result in the U-series being in disequilibrium. Where this involves short-lived daughters, disequilibrium with the nearest long-lived parent will also be short-lived. For example, ^{226}Ra will usually be in equilibrium with its short-lived daughters ^{214}Pb and ^{214}Bi. Disequilibria between long-lived members such as ^{230}Th (half-life 75380 years) and ^{226}Ra (half-life 1600 years) will take many thousands of years to resolve. In these cases the activity must be measured using photo peaks from the radionuclide itself, or its short-lived daughters. Because secular disequilibrium is typically caused by the mobilisation of ^{234}U and ^{226}Ra, the following energies are key to detect radioactive disturbance: 63 keV and 92 keV (to infer ^{234}U through ^{234}Th), 186 keV (to quantify ^{226}Ra) and 46 keV (to quantify the end member ^{210}Pb). There are non-trivial issues associated with these photo peaks that need to be solved in order to determine the activity of ^{234}Th, ^{226}Ra and ^{210}Pb (see sec 6.1 and 6.2). A major obstacle in determining the complete ^{238}U series is the absence of significant gamma emissions from ^{230}Th. In samples that have been isolated on timescales of tens of thousands of years, ^{230}Th will be in secular equilibrium with its daughter radionuclide ^{226}Ra and can thus be determined via the ^{226}Ra emission. On shorter timescales, potential disequilibria between ^{230}Th and ^{226}Ra are a significant source of uncertainty.

6.1 Correcting peak interference

At 92 keV the gamma peak of ^{234}Th is interfered by x-rays and by other gamma peaks including the 93.3 keV thorium line (Huy and Luyen, 2005; see Appendix D for details). In addition, for Ge detectors there is a contribution below the photopeak from multiple Compton scattering where the interaction probability ratio for photoelectric effect and Compton scattering is detector dependent. There is also background from Comptons from higher energy peaks so that, effectively, the background at 92-93 keV is a continuum with a small step at each peak (Fig. 4). It is good practice to first collect some spectra from Th-rich samples to define position and characteristics of the peaks near 92 keV so that energies and FWHMs can be fixed when deconvoluting the peak region (Fig. 4). All these non-trivial issues may rule out the use of the 92 keV peak for quantifying ^{234}Th, leaving us with its 63 keV peak that, however, overlaps with a ^{232}Th decay peak at 63.8 keV (Pγ=0.263%; see also https://www.nndc.bnl.gov/). For the purpose of data robustness both peaks are, ideally, analysed and compared (Fig. 5). This process can be more straightforward if a detector with excellent low-energy resolution is used.

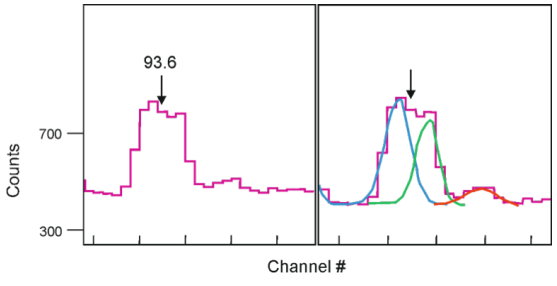

Fig. 4. Fitting the 92-93 keV energy peak using the g3 software (see Appendix D for details). Left: typical 93 keV peak; right: deconvolution of peak resulting in 3 different peak functions (blue, green, orange).

https://doi.org/10.5194/gchron-2021-32
Preprint. Discussion started: 3 November 2021

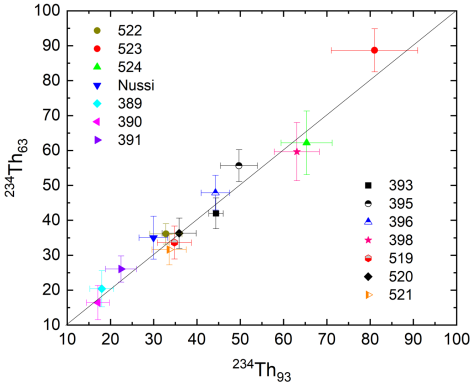

Fig. 5. Testing the correction of the 63 keV and 92 keV energy lines (Abdualhadi et al., 2018). Symbols represent sample codes of 14 samples originating from different geographical regions and environments.

At 186 keV the gamma peaks of ^{226}Ra and ^{235}U overlap. There are three ways to handle this:

(1) subtracting the ^{235}U portion from the total activity deduced from the 186 keV peak. This is achieved by calculating the natural isotopic ratio of ^{238}U and ^{235}U by taking into account atomic mass, Avogardro constant, decay rate and half live of each radionuclide. This results in 58% of the counts in the 186 keV peak emitted by ^{226}Ra and 42% emitted by ^{235}U. Assuming secular equilibrium between ^{238}U and ^{226}Ra these percentages are constant and can be used as nominal factor to correct the interference at 186 keV.

(2) calculating the ^{226}Ra activity by including other gamma peaks (e.g., de Corte et al., 2005). With this method the ^{235}U activity is directly inferred from its peak at 144 keV or indirectly from the ^{234}Th peak at 63 keV. The method requires correction of peak interference at 63 keV and of true coincidence summing as well as adoption of the natural isotopic ratio of ^{238}U and ^{235}U. Its advantage is that secular equilibrium is assumed only between ^{238}U and its immediate daughter ^{234}Th.

(3) bypassing correction procedures by sealing the sample against ^{222}Rn escape (as indicated in section 4) and determining ^{226}Ra via the emissions from its short-lived daughters ^{214}Pb (352 keV) and/or ^{214}Bi (609 keV). Note however that ^{214}Bi emissions can be significantly affected by coincidence summing.

We have compared approaches (2) and (3). The results are ambiguous (Fig. C1) suggesting that correction (2) is insufficient to accurately determine the ^{226}Ra activity (see Appendix D for details).

6.2 Correcting self-absorption

A fraction of gamma photons generated by radioactive decay are lost by absorption within the sample before reaching the detector. The extent of the losses will be controlled by the sample mass, measurement geometry, and the gamma ray attenuation coefficient of materials within the sample. They will generally be relatively small at high photon energies but much more significant at low photon energies. A semi-empirical formula for estimating the losses is

https://doi.org/10.5194/gchron-2021-32
Preprint. Discussion started: 3 November 2021

$$N = N_o \, e^{-k\hat{\mu}m}$$

where N is the number of photons actually detected, N_0 the number of photons that would have been detected in the absence of self-absorption, m is the mass of the sample, $\hat{\mu}$ the material gamma ray mass attenuation coefficient, and k a parameter characterising the geometry of the sample (Appleby et al., 1992). Values of the attenuation coefficient can be determined empirically using the Beer-Lambert law (equation A1) by measuring the reduction in intensity when a collimated beam of gamma rays is passed through the sample (transmission method). Table 4 lists empirically determined intensity reduction values (I/I_0) for a number of samples with different densities and chemical properties at photon energies in the range 32 keV to 121 keV. Differences between samples are relatively small at photon energies greater than 60 keV, but may be significant at low photon energies. More advanced approaches are available using the Monte Carlo N-Particle (MCNP) transport code which effectively simulates the interaction of gamma rays emitted in random direction by a sample of known density and chemical composition with the detector (for details see Abdualhadi et al., 2018). Where the sample has a known chemical composition estimates of the attenuation coefficient can be made using information available in published databases (see Appendix A).

Many studies have addressed the issue of self-absorption (e.g. Huy and Luyen, 2005; Aguiar et al., 2006; Khater and Ebaid, 2008; Kaminski et al., 2014; Barrera et al., 2017), each employing a slightly different method depending on available tools in the respective laboratory. Often, experimental work (e.g., Huy and Luyen, 2005; Aguiar et al., 2006; Khater and Ebaid, 2008) is combined with Monte Carlo-based model work (e.g., Huy et al., 2013; Bruggeman et al., 2016).

Table 4. Transmitted intensities of gamma rays (I/I_0) for sandy samples with different densities (and chemical composition). I/I_0 was calculated using eq S1. Gamma energy (E_γ, keV) of points sources are 32 (^{137}Cs), 39 (^{152}Eu), 59 (^{241}Am), 80 (^{133}Ba) and 121 (^{152}Eu) (Abdualhadi, 2016).

Sample code	Density (g cm^{-3})	E_γ (keV)				
		32	39	59	80	121
		I/I_0	I/I_0	I/I_0	I/I_0	I/I_0
LV393	1.47	0.13 ± 0.02	0.27 ± 0.01	0.50 ± 0.02	0.61 ± 0.02	0.69 ± 0.03
LV519	1.49	0.13 ± 0.02	0.29 ±0.01	0.52 ± 0.02	0.63 ± 0.02	0.70 ± 0.03
LV390	1.51	0.20 ± 0.02	0.32 ± 0.02	0.55 ± 0.02	0.65 ± 0.02	0.67 ± 0.03
LV520	1.66	0.10 ± 0.02	0.26 ± 0.01	0.52 ± 0.02	0.65 ± 0.02	0.68 ± 0.03
LV396	1.81	0.09 ± 0.02	0.23 ± 0.01	0.51 ± 0.02	0.61 ± 0.02	0.68 ± 0.03

7 Summary

This is part 1 of our paper on the quantification of Uranium-series disequilibrium in natural samples. It focuses on basic principles for estimating contemporary dose rates using gamma spectrometry. We describe basics of gamma radiation and the penetration depth of this radiation in matter as a function of photon energy and material properties. The detectors suitable for detecting gamma-ray emissions in the typical range of 10-2600 keV (Fig. 1) are high-purity Germanium (HPGe) crystals operated at low temperature (Table 1). The fully absorbed gamma photons entering the detector crystal generate discrete full-energy peaks in the gamma spectrum that are specific to ^{40}K and the radioisotopes of the ^{238}U- and ^{232}Th-series. The analysis of these full-energy peaks accounts for the gamma-emission probability of the corresponding

https://doi.org/10.5194/gchron-2021-32
Preprint. Discussion started: 3 November 2021

radioisotope, the detector's efficiency and background at that energy and accompanying interactions between sample and detector. All together result in the choice of a number of photon peaks suitable for estimating the parent nuclide activities (Tables 2 and 3). For these peaks the simple comparison with a reference material of know activity (e.g., Volkegem loess) deliver accurate activities of individual radioisotopes, hence the parent nuclide, with an uncertainty of 3-6%.

The essential prerequisite of this approach is radioactive equilibrium, that is, all members of the ^{238}U series have the same activity. Since only samples that have been isolated for millions of years will be in secular equilibrium, most samples that are subject to dosimetric dating are likely to exhibit disequilibrium. The significance of this disequilibrium for the dose-rate estimate depends on the radioisotope involved and the duration of the process that leads to loss or gain of a ^{238}U series member. If disequilibrium is suspected, the photon peaks at 46, 63 and 92 keV and at 186 keV have to be analysed and this involves accounting for peak interference and self-absorption both being well-known issues of gamma-spectrometry. Advanced approaches are today available using the Monte Carlo N-Particle (MCNP) transport code which effectively simulates the interaction between detector and gamma rays emitted in random direction by a sample of known density and chemical composition. This allows quantifying the activities of key members of the ^{238}U series required to calculate the historical dose rate by solving the Bateman equation. This will subject of part 2 of our paper.

8 Appendices

Appendix A: Penetration depth and attenuation of gamma rays

Depending on the photon energy, and characteristics of the material, gamma rays can penetrate objects to a depth of several centimetres, though the intensity (I) attenuates exponentially with distance (**x**) in accordance with the Beer-Lambert law

$$I = I_0 \, \mathrm{e}^{-\mu x} \qquad \text{(A1)}$$

The (linear) attenuation coefficient μ is a function of photon energy and material characteristics. The penetration depth is defined as the distance over which the intensity is reduced to a fraction 1/e (37%) of its initial value I_0 (that is, a 63% reduction) and is given by

$$\delta = 1/\mu. \qquad \text{(A2)}$$

The intensity reduces by 50% over a depth $\ln(2)/\mu = 0.69\,\delta$. Values of the mass attenuation coefficients given in the literature are usually expressed in terms of the mass attenuation coefficient, defined as

$$\hat{\mu} = \mu/\rho \qquad \text{(A3)}$$

where ρ is the mass density. For example, the mass attenuation coefficient for 1 MeV photons in SiO_2 is 0.0637 cm^2 g^{-1}; since the density is 2.32 g cm^{-3}, the linear attenuation coefficient is 0.148 cm^{-1}. The penetration depth (63% reduction) is thus 6.8 cm and is 4.7 cm for a 50% reduction. Values of $\hat{\mu}$ at other photon energies or for other materials can be found in the literature (e.g., Hubbell, 1983) or from online databases (https://dx.doi.org/10.18434/T4D01F)

https://doi.org/10.5194/gchron-2021-32
Preprint. Discussion started: 3 November 2021

Appendix B: Measurement geometry

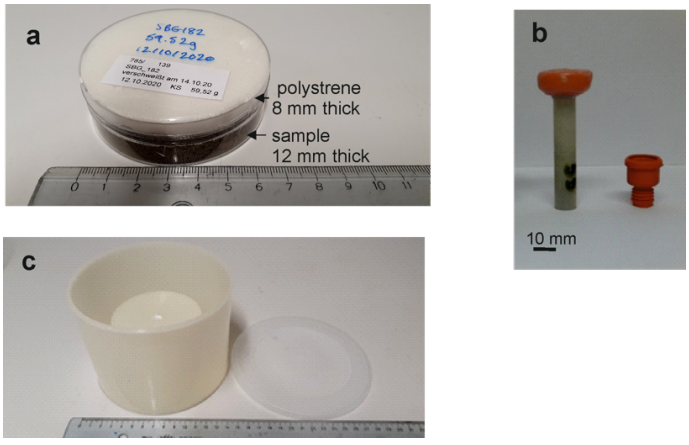

Fig. B1. Sample holders typically used for measuring a gamma spectrum. (a) – cylinder; (b) – well tube; (c) – Marinelli beaker.

Fig. B2. Samples mixed with wax and casted in three different geometries (Photo kindly provided by Vicki Hansen, DTU).

Appendix C: Efficiency calibration and reference material

The peak area given by most software will include emissions from both the sample and the background counts from the environment in which the detector is used and the detector itself. These can be determined by carrying out background counts without a sample being present. Writing N_T for the gross counts in a peak given by the software and N_B for the

https://doi.org/10.5194/gchron-2021-32
Preprint. Discussion started: 3 November 2021

number of counts attributable to the background, the number attributable to the sample itself will be $N = N_T - N_B$. The activity of the radionuclide giving rise to those emissions can be calculated using the formula

$$A = \frac{N}{mTP_\gamma \eta} \quad \text{(C1)}$$

where m is the mass of the sample, T the count time, P_γ the gamma emission probability, η a practical efficiency that takes account not only of the full energy efficiency of the detector at that energy, but also the effects of factors such as self-absorption, and where necessary, true coincidence summing (Gilmore, 2008). The effects of self-absorption can be minimised by limiting the sample size.

A procedure that avoids many difficulties is to use a reference material of known activity with similar self-absorption characteristics to that of the sample, having exactly the same geometry. Activities in the sample can then be calculated by direct comparison with the reference material using the equation

$$A_{sample} = \frac{\left[N/(mT)\right]_{sample}}{\left[N/(mT)\right]_{reference}} \times A_{reference} \quad \text{(C2)}$$

Equation (C2) is valid on a peak by peak basis which requires that $A_{reference}$ is known for each peak of interest. Alternatively, if $A_{reference}$ is only known for ^{238}U, all members of the ^{238}U series in both reference material and unknown sample have to be in secular equilibrium. In this case the activity can in principle be determined using any of the photon peaks listed in Table 2. In practice some peaks are more suitable then others depending on the sensitivity of the peak to the sample's Z and density and on detector-specific parameters such as energy resolution, full-energy peak efficiency.

Non-certified reference samples

Two loess samples, namely Volkegem (De Corte et al., 2007) and Nussi (Preusser and Kasper, 2001) have previously been proposed as suitable reference materials. Loess is a sedimentary deposit resulting from the accumulation of wind-blown dust. Typically, a loess deposit is several meters thick and composed of 20-40 micron grains. The grains comprise minerals such as feldspars, quartz and heavy minerals in percentages representative for the provenance areas. Loess is mostly transported over long distances and over large areas carrying hence the signature of a significant proportion of earth surface which is then homogeneously distributed in the accumulation. In fact, while grain size may vary between outcrops, radionuclide activity concentrations are strikingly similar (see e.g., Scheidt et al., 2021 for the Carpathian loess; Roberts et al., 2003 for North American loess; Sauer et al., 2016 for central European loess; Lü et al., 2020 for Chinese loess).

Volkegem - this material is derived from a loess deposit in Belgium (De Corte et al., 2007).

Nussi – this material is derived from a loess deposit in southern Germany (Preusser and Kasper, 2001). The material is registered with the International Association of Geoanalysts (http://www.geoanalyst.org) as 'Loess-1 GeoPT13' with assigned chemical values for all low-mass elements (Potts et al., 2003).

Both samples have been tested in several luminescence laboratories. Here we provide details for the Volkegem material - see Table C1.

https://doi.org/10.5194/gchron-2021-32
Preprint. Discussion started: 3 November 2021

Table C1. The Volkegem loess: activity concentrations (Bq kg^{-1}) determined in different laboratories using different methods.

Laboratory	Method	Ref material	^{238}U	^{235}U	U	^{226}Ra	^{232}Th	^{40}K	Reference
Ghent	multiple	n/a	34.5±1.5	1.59±0.09	36.1±1.7	34.1±2.3	42.2±2.5	497±45	De Corte et al., 2007
Liverpool	γ-spec; eq. S4	IAEA-375	38.8±2.1	-	-	-	44.4±0.7	571±13	This study
Aberystwyth	ICP-MS	-	37.8±0.5	-	-	-	44.3±1.5	543±6	Pers. com., Geoff Duller, June 2017
Dresden	Trans-mission	-	43±5	-	-	42.2±2.8	-	535±56	Pers. com., Detlev Degering, June 2017
Risoe	γ-spec.	BL-5, OKA-2 and K_2SO_4	37.8±0.7	-	-	42.8±0.2	44.2±0.5	570±5	Murray et al. (2018)
Salzburg	γ-spec; eq. S3	QCYB41	38.4±0.7	-	-	48.2±6.2	40.4±1.5	556±20	This study

Certified reference material

Table C2 lists a number of materials commonly used for efficiency calibration. It should be noted that some of these materials entail problems; for instance, some radionuclides included in the QCYK multi-nuclide reference material exhibit true coincidence summing when measured close to the detector (Gilmore, 2008) and this limits the usage of some energy lines.

Table C2. Reference material commonly used for efficiency calibration. Activities are given in Bq kg^{-1}. R=recommended; C=certified; I=information.

Code	Descrip-tion	^{238}U	^{226}Ra	^{232}Th	^{40}K	Reference	Re-liability
IAEA 314	Inorganic stream sediment	-	733±55	68±4	-	https://nucleus.iaea.org/sites/ReferenceMaterials/Pages/IAEA-314.aspx	R
IAEA 375	Inorganic soil	24.4±5.4	20±2	20.5±1.4	425±8	https://nucleus.iaea.org/sites/ReferenceMaterials/Pages/IAEA-375.aspx	R
IAEA 448	Organic soil	49.2±0.9	1905±260 (C)	13.4±1.1	234±12	https://nucleus.iaea.org/sites/ReferenceMaterials/Pages/IAEA-448.aspx	C and I
IAEA-RGU-1	Uranium ore, diluted	4941±99	-	-	-	https://nucleus.iaea.org/sites/ReferenceMaterials/Pages/IAEA-RGU-1.aspx	C
IAEA-RGTh-1	Inorganic ores	78±6	-	3250±90	6.3±3.2 (I)	https://nucleus.iaea.org/sites/ReferenceMaterials/Pages/IAEA-RGTh-1.aspx	R
Nussi	loess	33.5±1.1	18.8±1.9	30.08±1.38	299.10±0.12	Converted from Preusser and Kasper (2001) using the Avogadro constants	I
Volkegem	loess	34.5±1.5	34.1±2.3	42.2±2.5	497±45	De Corte et al. (2007)	I
BL-5	Uranium ore	-	$857x10^3$±3 $8x10^3$	-	-	https://www.nrcan.gc.ca/our-natural-resources/minerals-mining/mining-resources/bl-5-certificate-analysis/8115	C
OKA-2	Thorium ore	888±33	-	$117.4x10^6$±2. $3x10^4$	?	https://www.nrcan.gc.ca/our-natural-resources/minerals-mining/mining-resources/oka-2-certificate-analysis/8135	C

https://doi.org/10.5194/gchron-2021-32
Preprint. Discussion started: 3 November 2021

QCYB41	Multinuclide solution	-	-	-	-	Eckert and Ziegler (2016)	C
K_2SO_4	Purity given as 100.4%	-	-	-	$14.23x10^3 \pm 0.03x10^3$	Murray et al. (2018)	I

We compared two different efficiency calibration methods using the coaxial (n) detector of this study described in Table 1: one uses the multi-nuclide reference solution QCYB41 and follows equation C1. The other one is based on the direct comparison with the Volkegem reference material using equation C2. 81 samples with different activities originating from geochemically variable environments were used for the comparative study. Almost perfect agreement exists for energy lines 1460, 338, 352, 609, 911 and 46 keV. Systematic differences appear for energy lines 63 keV and 238 keV (Mauz et al., in review). These results suggest that accurate activity data are obtained from the simple comparison with the non-certified Volkegem reference material as long as suitable energy peaks are selected to determine the parent nuclide.

Software suitable to analyse full-energy peak efficiency

Canberra LabSOCS application note; http://canberra.com/literature/application-notes.asp

Ortec ANGLE user guide: https://www.ortec-online.com/-/media/ametekortec/manuals/angle-mnl.pdf?la=en&revision=735a4dc6-825e-4162-b8c2-79309ec76842.

Appendix D: Peak interference

Overlaps between neighbouring peaks will occur where photon peaks are separated by less than around 2.5 times the FWHM value, that is, between 4-5 keV, for example, the ^{226}Ra peak at 186.2 keV which is separated from the nearby ^{235}U peak at 185.7 keV by just 0.5 keV. Most modern high-resolution detectors are incapable of separating them and will record them as a single peak. Where the separation is greater and two overlapping peaks can be distinguished, it may be possible to apportion the total area between the two. One method is to assign fractions based on the areas below the lower peak and above the upper peak.

Although ^{238}U does not have significant gamma emissions itself, it will normally be in radioactive equilibrium with its short-lived daughter ^{234}Th (half-life 24.1 days). ^{234}Th has two significant photon peaks, at around 63.3 keV and 92.6 keV, though both are in fact composite peaks. The 92.6 keV gamma line includes two separate ^{234}Th peaks at 92.4 keV and 92.8 keV, a small ^{235}U peak at 93.4 keV, two ^{231}Th peaks, at 92.3 keV and 93.0 keV and x-rays (Huy and Luyen, 2005). ^{226}Ra activity is best determined using one of the peaks of its short-lived daughter radionuclides ^{214}Pb or ^{214}Bi. ^{235}U may be determined either via its peaks at 144 keV or 205 keV, or in natural samples, from the established activity ratio with ^{238}U. See also De Corte et al. (2005) and https://www.nndc.bnl.gov/. In practice, the methods available for correcting the 186 keV emission deliver ambiguous results (e.g., Fig. C1). The correction procedure should therefore be replaced by the use of a software in which a detailed detector characterisation is combined with the MCNP Monte Carlo modelling code (see Appendix C for software references).

https://doi.org/10.5194/gchron-2021-32
Preprint. Discussion started: 3 November 2021

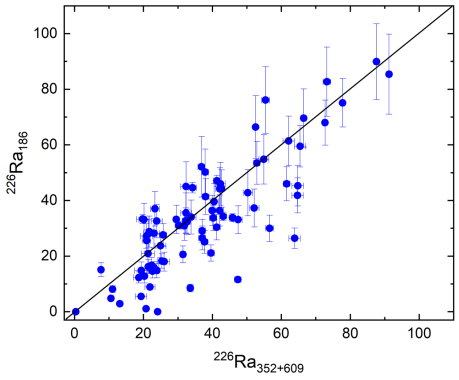

Fig. D1. Comparing activity data (Bq kg^{-1}) obtained from the photon peak at 186 keV. Each blue dot represents a sample in relation to the 1:1 black line. $^{226}Ra_{186}$ activity is derived from equation C1 corrected for the activity of ^{235}U directly inferred from its peak at 144 keV and plotted versus the weighted mean of activities derived from the ^{226}Ra daughters emitting 352 and 609 keV.

Software suitable to analyse overlapping photon peaks
https://radware.phy.ornl.gov/gf3/gf3.html

9 Author contributions

BM designed the work and wrote the text; PA and PN oversaw text and figures dealing with gamma radiation, instruments and associated equations.

10 Competing interest

The authors declare that they have no conflict of interest.

11 Acknowledgements

This work was facilitated by Sumia Abdualhadi who studied the quantification of U-series disequilibrium using gamma spectrometry in her PhD. BM is grateful for the continuous support provided by Alexander Hubmer and Chiara Bahl (University of Salzburg).

12 References

Abdualhadi, S.A., Mauz, ,B., Joss, S.D.T, Nolan, P.: Detecting and quantifying uranium-series disequilibrium in natural samples for dosimetric dating applications. Radiation Measurements 114, 25-31, https://doi.org/10.1016/j.radmeas.2018.04.011, 2018.

Abdualhadi, S.A.: Quantifying disequilibrium in U-series decay using high-purity germanium spectrometry. PhD thesis, University of Liverpool, 2016.

https://doi.org/10.5194/gchron-2021-32
Preprint. Discussion started: 3 November 2021

Aguiar, J.C., Galiano, E., Fernandez, J.: Peak efficiency calibration for attenuation corrected cylindrical sources in gamma ray spectrometry by the use of a point source. Appl. Radiation and Isotopes 64, 1643-1647, doi:10.1016/j.apradiso.2006.05.014, 2006.

Appleby P.G., Richardson, N., Nolan, P.J.: Self-absorption corrections for well-type germanium detectors. Nucl. Inst. and Methods B, 71,228-233, 1992.

Barrera, M., Suarez-Llorens, A., Casas-Ruiz, M., Alonso, J.J., Vidal, J.: Theoretical determination of gamma spectrometry systems efficiency based on probability functions. Application to self-attenuation correction factors. Nuclear Instruments and Methods in Physics Research A, 31–39, http://dx.doi.org/10.1016/j.nima.2017.02.052, 2017.

Bruggeman, M., Verheyen, L., Vidmar, T., Liu, B.: Assessing sample attenuation parameters for use in low-energy efficiency transfer in gamma-rayspectrometry. Appl. Radiation and Isotopes 109, 547-550, http://dx.doi.org/10.1016/j.apradiso.2015.11.077, 2016.

De Corte, F., Vandenberghe, D., Hossain, S.M., De Wispelaere, A., Buylaert, J.-P., Van den Haute, P.: Preparation and characterization of loess sediment for use as a reference material in the annual radiation dose determination for luminescence dating. Journal of Radioanalytical and Nuclear Chemistry 272, 311–319, DOI: 10.1007/s10967-007-0522-5, 2007.

De Corte, F., Umans, H., Vandenberghe, D., De Wispelaere, A., Van den haute, P.: Direct gamma-spectrometric measurement of the ^{226}Ra 186.2 keV line for detecting ^{238}U/^{226}Ra disequilibrium in determining the environmental dose rate for the luminescence dating of sediments. Appl. Radiation and Isotopes 63, 589-598, doi:10.1016/j.apradiso.2005.05.008, 2005.

Degering, D., Degering, A.: Change is the only constant - time-dependent dose rates in luminescence dating. Quat. Geochron. 58, 101074, https://doi.org/10.1016/j.quageo.2020.101074, 2020.

Eckert & Ziegler (Deutsche Akkreditierungsstelle), 2016. Calibration certificate for Dept of Physics, Biophysics and Chemistry and Physics of the Materials, University of Salzburg, unpublished document.

Gilmore, G.: Practical gamma spectrometry. Wiley, West Sussex, 2008.

Guibert, P and Schvoerer, M.: TL Dating: Low background gamma spectrometry as a tool for the determination of the annual dose. Nucl. Tracks Radiat. Meas. 18, ½, 231-238, 1994

Hubbell J.H.: Photon Mass Attenuation and Energy-absorption Coefficients from 1 keV to 20 MeV. Int. J. Appl. Radiat. Isot. 33,1269-1290, 1983.

Hubbell, J.H., Seltzer S.M.: NIST Standard Reference Database 126. Tables of X-Ray Mass Attenuation Coefficients and Mass Energy-Absorption Coefficients from 1 keV to 20 MeV for Elements Z = 1 to 92 and 48 Additional Substances of Dosimetric Interest. Radiation Physics Division, PML, NIST, https://dx.doi.org/10.18434/T4D01F, 2004.

Huy, N.Q., Binh, D.Q., An, V.X., Hong Loan, T.T., Thanh Can, N.: Self-absorption correction in determining the ^{238}U activity of soil samples via 63.3 keVgamma ray using MCNP5 code. Appl. Radiation and Isotopes 71, 11-20, http://dx.doi.org/10.1016/j.apradiso.2012.09.004, 2013.

Huy, N.Q., Luyen, T.V.: A method to determine 238U activity in environmental soil samples by using 63.3-keV-photopeak-gamma HPGe spectrometer. Appl. Radiation and Isotopes 61, 1419-1424, doi:10.1016/j.apradiso.2004.04.016, 2005.

Kaminski, S., Jakobi, A, Wilhelm, Chr.: Uncertainty of gamma-ray spectrometry measurement of environmental samples due to uncertainties in matrix composition, density and sample geometry. Appl. Radiation and Isotopes 94, 306-313, http://dx.doi.org/10.1016/j.apradiso.2014.08.008, 2014.

Khater, A.E.M., Ebaid, Y.Y.: A simplified gamma-ray self-attenuation correction in bulk samples. Applied Radiation and Isotopes 66, 407–413, doi:10.1016/j.apradiso.2007.10.007, 2008.

Knoll, G.F.: Radiation detection and measurement. Wiley & Sons, Inc., 2010.

https://doi.org/10.5194/gchron-2021-32
Preprint. Discussion started: 3 November 2021

Lü, T., Sun, J., Feathers, J.K., Sun, D.: Spatiotemporal variations and implications of luminescence sensitivity of quartz grains on the Chinese Loess Plateau since the last interglaciation. Quaternary Research doi:10.1017/qua.2020.53, 2020.

Mauz, B., Hubmer, A., Bahl, C., Lettner, H., Lang, A.: Comparing two efficiency calibration methods commonly used in gamma spectrometry. Ancient TL, in review, 2021.

Murray, A., Buylaert, J.-P., Thiel, C.: A luminescence dating intercomparison based on a Danish beach-ridge sand. Radiation Measurements 81, 32-38, http://dx.doi.org/10.1016/j.radmeas.2015.02.012, 2015.

Murray, A., Helsted, L.M., Autzen, M., Jain, M., Buylaert, J.-P.: Measurement of natural radioactivity: Calibration and performance of a high-resolution gamma spectrometry facility. Radiation Measurements 120, 215-220, https://doi.org/10.1016/j.radmeas.2018.04.006, 2018.

Murray, A.S., Aitken, M.J.: Analysis of low-level natural radioactivity in small mineral samples for use in thermoluminescence dating, using high-resolution gamma spectrometry. Appl. Radiat. Isot. 39,2, 145-158, 1988.

Murray, A.S., Marten, R., Johnston, A., Martin, P.: Analysis of naturally occurring radionuclides at environmental concentrations by gamma spectrometry. Journal of Radioanalytical and Nuclear Chemistry, 115, 263-288, 1987.

Preusser, F., Kasper, H.U.: Comparison of dose rate determination using high-resolution gamma spectrometry and inductively coupled plasma-mass spectrometry. Ancient TL 19, 19-23, 2001.

Readhead, M.L.: Thermoluminescence dose rate data and dating equations for the case of disequilibrium in the decay series. Nucl. Tracks Radiat. Meas., 13, 197-207, 1987.1987.

Roberts, H.M., Muhs, D.R., Wintle, A.G., Duller, G.A.T., Arthur Bettis III, E.: Unprecedented last-glacial mass accumulation rates determined by luminescence dating of loess from western Nebraska. Quaternary Research 59, 411–419, doi:10.1016/S0033-5894(03)00040-0, 2003.

Sauer, D., Kadereit, A., Kühn, P., Kösel, M., Miller, C.E., Shinonaga, T., Kreutzer, S., Herrmann, L., Fleck, W., Starkovich, B.M., Stahr, K.: The loess-palaeosol sequence of Datthausen, SW Germany: Characteristics, chronology, and implications for the use of the Lohne Soil as a marker soil. Catena 146, 10-29, http://dx.doi.org/10.1016/j.catena.2016.06.024, 2016.

Scheidt, S., Berg, S., Hambach, U., Klasen, N., Pötter, S., Stolz, A., Veres, D., Zeeden, D., Brill, D., Brückner, H., Kusch, S., Laag, C., Lehmkuhl, F., Melles, M., Monnens, F., Oppermann, L., Rethemeyer, J., Nett, J.J.: Chronological assessment of the Balta Alba Kurgan loess-paleosol section (Romania) – A comparative study on different dating methods for a robust and precise age model. Front. Earth Sci. 8:598448, doi: 10.3389/feart.2020.598448, 2021.